PAPER • **OPEN ACCESS**

Investigation of multi-tip large area emitters using computerized field emission projector

To cite this article: S V Filippov *et al* 2019 *IOP Conf. Ser.: Mater. Sci. Eng.* **525** 012051

IOP Conf. Series: Materials Science and Engineering **525** (2019) 012051 doi:10.1088/1757-899X/525/1/012051

Investigation of multi-tip large area emitters using computerized field emission projector

S V Filippov[1], A G Kolosko[1], R M Ryazanov[2], E P Kitsyuk[2] and E O Popov[1]

[1]Ioffe Institute, ul. Polytechnitscheskaya 26, St.-Petersburg, 194021, Russia
[2]Scientific-Manufacturing Complex "Technological Centre", Shokin Square, Bld. 1/7, Zelenograd, 124498, Russia

E-mail: s.filippov@mail.ioffe.ru

Abstract. The paper presents an original approach to the numerical analysis of emission patterns of the flat field emission projector. A system for testing and numerical characterization of the emission properties of field cathodes was developed. A sample of the multi-tip large area field emitter based on non-oriented carbon nanotubes grown on a tungsten substrate was studied by the emission glow pattern analysis.

1. Introduction

The development of manufacturing technologies for conducting nanoscale structures (carbon nanotubes, graphene plates, nano-diamonds, etc.) made it possible to use such structures as field sources of free electrons for the needs of vacuum micro- and nanoelectronics. Multi-tip emitters based on carbon nanotubes (CNT) have proven themselves in the best way. This is due to the high aspect ratio of CNTs, their high thermal conductivity and the ability to withstand high current densities (up to 10^7 A/cm^2).

Today, prototypes of devices using CNT-based emitters exist: vacuum electrodynamic tethers [1], compact mass spectrometers [2], vacuum sensors [3], medical tomographs [4] and etc. However, a number of related factors affecting emissions limit the stability and the lifetime of this type of field emitters. The distribution of the current loading over the set of individual nanoscale emission sites increases their individual stability, however, the stochasticity of the geometric parameters and the mutual position of the sites leads to the occurrence of explosive emission.

Investigation of the instability of the total emission current and its fluctuations of multi-tip field emitters requires observation of the state and evolution of their surface.

The main methods for obtaining information about the surface of a nanostructured emitter are scanning electron microscopy (SEM) [5], field emission scanning electron microscopy (FE-SEM) [6], field emission microscope with a scanning anode (SAFEM) [7]. However, the most accessible in terms of ease of data analysis and technical implementation is the method of direct observation of emission sites on the emitter surface – field emission projector (FEP) [8]. Computer processing of the glow patterns registered with the FEP, together with the registration and online processing of the field emitter current-voltage characteristics (IVC), opens up broad possibilities for obtaining information on the emission ability and the interaction of individual emission sites.

For example, in [9], digitized FEP luminescence patterns were used to calculate the field emission area of individual emission sites. In [10], instead of the luminescent coating on the anode, resistive PMMA thin film was used, which is sensitive to the flux of electrons emitting from the surface of the field cathode. Using this original technique, histograms of the distribution of microscopic emission sites

by heights were constructed. At the same time, SEM pictures were used for surface analysis and the IVC of the sample were recorded.

In [11], the YAG: Ce (yttrium aluminum garnet doped with cerium) coated with a Mo film was used as a fluorescent anode in FEP. Using FEP field emission properties of nanodiamond films were studied. Image analysis of individual emission sites made it possible to determine the nonlinear dependence of the effective emission area on the applied electric field. The effect of saturation of the emission current with increasing voltage for semiconductor emission structures was also demonstrated.

In [12], a computerized characterization system for multi-tip field emitters using FEP in conjunction with recording voltage and emission current levels is presented. It is proposed to use the total brightness of pixels corresponding to individual emission sites in the glow pattern as weighting factors when evaluating their individual emission current. The histograms of the pixel spread of individual emission sites over the current level were plotted.

In [13], ZnO nanowire circle pad arrays and coplanar-gate circle pad arrays were studied. From the luminescence patterns, the uniform distribution of the geometric characteristics of ZnO nanowires was determined. The macroscopic IVC in the Fowler-Nordheim coordinates made it possible to estimate the average field enhancement factor (FEF) of nanoscaled electron sources. A numerical estimate of the temporal stability of the emission current level was also made. The receipt of SEM pictures of the surfaces studied accompanied all measurements.

The purpose of this work was to study the emission properties of a multi-tip field emitter based on non-oriented CNTs using a computerized FEP.

2. Experimental

To study the emission properties of multi-tip field emitters, a unique experimental technique [14] was used. It is based on multichannel registration and online processing of field emission data. IVCs were recorded in the "fast" mode (one IVC for 20 ms) in two configurations: emitter with a metal anode (diode) and an anode coated with a conductive ITO layer on the glass and a layer of luminescent substance SVETOSOSTAV K-49. The latter configuration is equipped with a long-focus USB microscope mounted outside the vacuum chamber on a vacuum window and is called the FEP. The microscope records the glow patterns that appear on the luminescent coating and reflect the distribution of emission sites over the cathode surface. In fig. 1 schematically shows the device of the cathode systems of the measuring setup.

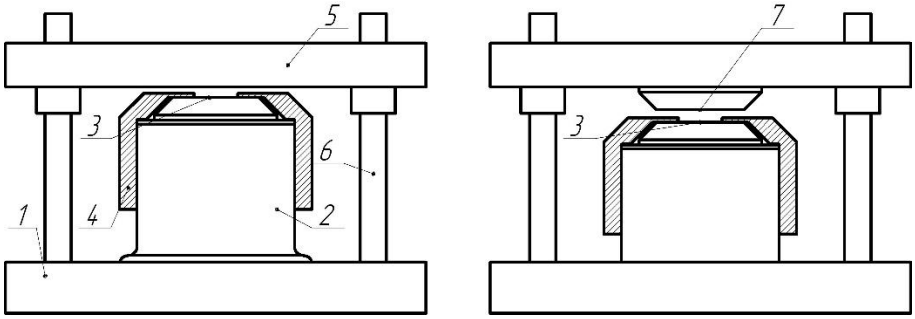

Figure 1. Scheme of experimental setup: (a) diode configuration and (b) FEP. 1 – Base, 2 – cathode holder, 3 – emitter on the substrate surface, 4 – guarding diaphragm, 5 – glass covered with ITO and luminescent powder, 6 – isolation stands, 7– tantalic anode.

The developed procedure for characterization of emitters is carried out in several stages:

1. Determination of the voltage of the emission current occurrence (above a given level, in our case it is 100 nA).
2. IVC registration with a maximum emission current at level of 10 μA or 100 μA, or 1 mA.

3. Recording the time dependence of the current and voltage levels during the so-called sample training (activation and aging of the emitter surface under the influence of a high electric field in diode configuration with a metal anode). Estimating of the maximum emission current achievable at sample training.

4. Determination of the voltage of the emission current occurrence of the trained sample.

5. IVC registration at stable level of the pulse amplitude of the emission current of 10 μA or 100 μA, or 1 mA.

6. Evaluation of the temporal stability of the emitter at current level of 1 mA.

7. Determination of the effective parameters of the sample - the emission area (A_{eff}) and the field enhancement factor (β_{eff}) with a stable current level of 1 mA, the construction of histograms of fluctuations of these parameters.

8. Characterization of the change in the emissivity of the sample with a sequential increase and decrease in the voltage level: registration of the change in the shape of the IVC with a smooth change in U and registration of the kinetics of a change in the current level I with a step change in U.

9. Replacing the metal anode with an anode with luminescent layer (FEP) and registering the pattern of emission site distribution over the cathode surface.

10. Determining the number and location of emission sites, their maximum emissivity and construction a histogram of the distribution of brightness sites.

11. The calculation of the local FEFs of the found sites and plotting corresponding histogram.

12. Construction of histograms of emission sites distribution over the cathode surface, numerical evaluation of its uniformity.

The studied sample of a multi-tip field cathode consisted of non-oriented CNTs. Tungsten was used as a substrate, on the surface of which thin metallic layers of Ti (10 nm thick) and Ni (2 nm thick) were deposited. These layers served as a catalyst for the synthesis of CNT by the PECVD method. The synthesis took place at the following parameters: temperature 680 °C, pressure 2 Torr, synthesis time 10 min. A mixture of Ar, H_2, C_2H_2, NH_3 was fed into the chamber. The diameter of the grown CNTs was 10–20 nm, the length was up to 3 μm. Figure 2 shows SEM images of a slice of the substrate with CNTs grown on it.

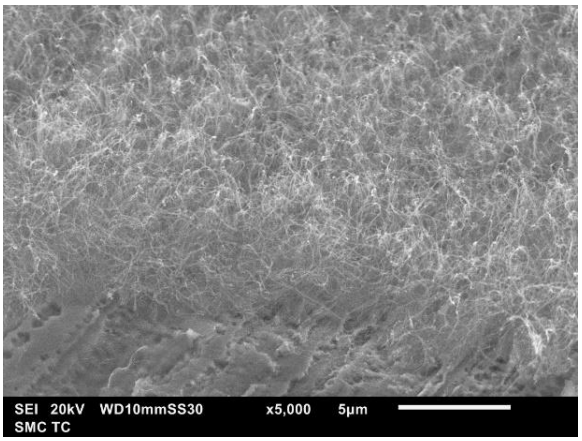

Figure 2. SEM image of the emitter surface at 45˚ angle.

3. Results

Before measuring the main emission characteristics of an as-prepared emitter, a high-voltage training procedure was required to activate and clean the surface of emission sites, as well as to shorten the highest and most unstable emission sites with a vacuum discharge. For this, a diode configuration with a flat metal anode and an interelectrode distance of 650 μm was used (taking into account the thickness of the metal diaphragm pressing the sample).

The change in the state of the emitter as a result of training is characterized by a change in the voltage value corresponding to the appearance of the emission current against the background of the noise of the measurement setup, as well as the IVC with a current amplitude of 1 mA (see Fig. 3a). The voltage of the emission of the as-prepared sample was U_{th0} = 350 V for current in I_{app} ~ 100 nA, and for the trained sample - U_{th0} = 900 V.

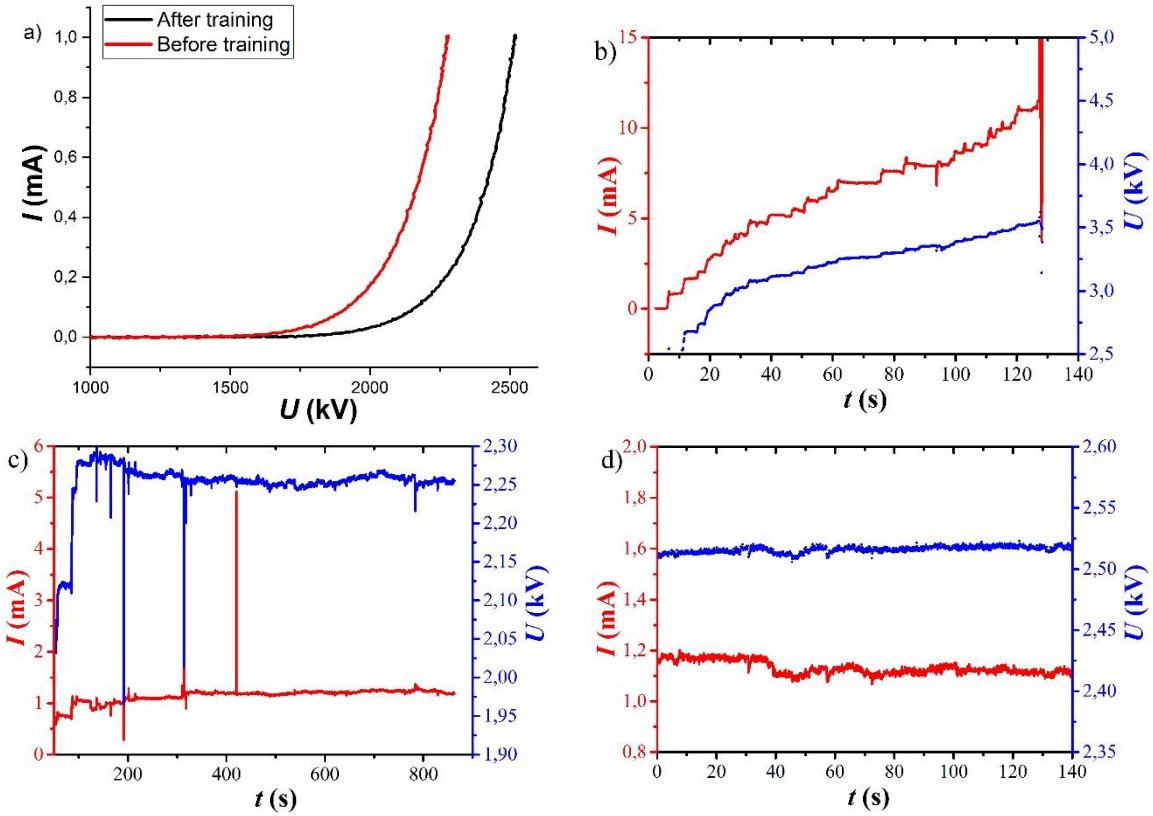

Figure 3. Emitter characteristics change due to high voltage training procedure: a) IVC of the emitter before and after training, b) changes in the amplitude of voltage pulses and corresponding emission current pulses during sample training, c), d) temporal stability of the emitter current at 1 mA before and after training.

Fig. 3b shows the process of training of the sample (the dependence of the current level on time). The maximum current reached during training was 11.5 mA. Above this level, discharges observed in the form of flashes in the interelectrode space steadily appeared, and the system could not maintain emission at a given current level.

Fig. 3 c, d represents the time dependences of the current and voltage levels recorded before and after training the sample at a current level of 1 mA. Sharp current level surges correspond to short-term vacuum discharges, because of which the highest emission sites were destroyed. The threshold voltage of the sample increases because of this, the total current decreases, but the probability of a vacuum discharge is reduced and the temporal stability of electron emission increases.

After activation of the emitter surface, the stability of its emission current over time was estimated (see Fig. 3d). Stability was assessed using the formula:

$$S = \frac{I_{max} - I_{min}}{I_{orig}} \cdot 100\%$$

where I_{max} and I_{min} are the maximum and minimum levels during the observation of current stability, respectively, and I_{orig} is the initial current level.

At amplitude of current pulses of 1 mA in 10 minutes, the stability S=14% was obtained.

The effective parameters of the emitter were estimated at stable current level from IVC in the Fowler – Nordheim coordinates (IVC-FN), [15]. Figure 4 presents the statistics of fluctuations of the effective enhancement factor β_{eff}, which indirectly characterizes the spread of emission characteristics over the sample surface [16]. As the voltage level increases, the β_{eff} values shift towards to lower values, which is explained by the inclusion of lower emission sites in the emission process.

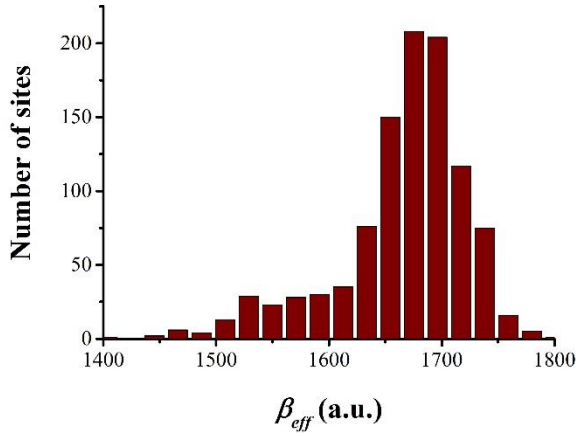

Figure 4. Histogram of fluctuations of the effective field enhancement factor of a CNT emitter at 200 μA current level.

The mean values of the parameters were as follows: for a current level of 1 mA: $S_{eff} \sim 5.0 \cdot 10^4$ nm^2 and $\beta_{eff} \sim 1520$, and for a current level of 200 μA: $S_{eff} \sim 4.8 \cdot 10^4$ nm^2 and $\beta_{eff} \sim 1650$.

In Fig. 5 shows the IVC for the current level of 200 μA and the corresponding trend line. Note that all registered in the fast mode IVC pass the Forbes test for compliance of the experimental data with "pure" field emission [17].

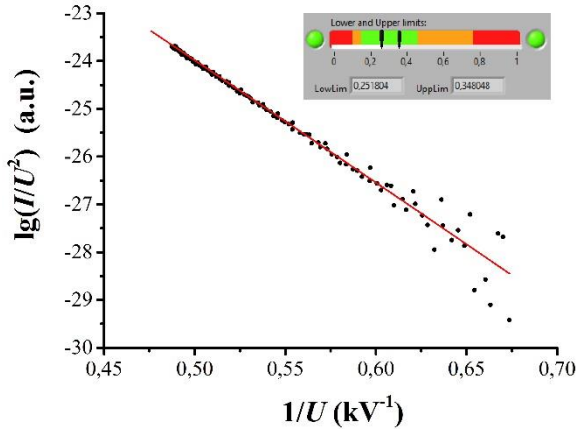

Figure 5. Estimation of the effective parameters from the IVC-FN (200 μA current level).

Figure 6 demonstrates the dynamic characteristics of the change in the emissivity of the sample with a stepwise increase and decrease in the voltage level. At the same time, there is an exponential increase and decrease in the level of the emission current when the amplitude of impulses of applied voltage reaches a new level. A cyclic change in the IVC shape is also observed, which is associated with a

change in the concentration of volatile products in the interelectrode space and on the cathode surface [18].

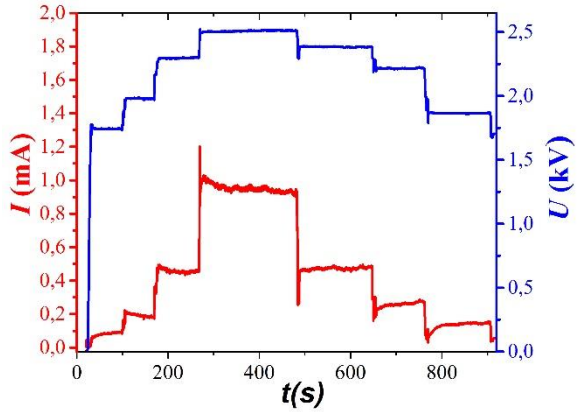

Figure 6. Dynamic characteristics of the change in the emissivity of the sample with a step increase and decrease in the voltage level.

The distribution of emission sites over the cathode surface and their local emission characteristics was studied in another diode system with a luminescent anode (FEP). Figure 7 presents the FEP emission pattern at different current levels (130, 250, 450 and 1000 μA).

Due to the instability of the luminescent coating to electron bombardment, obtaining high emission currents in such a configuration is impossible, moreover, at high currents, the image of emission sites begin to overlap and cease to be distinguishable. Therefore, the current levels in the study did not exceed 5 mA.

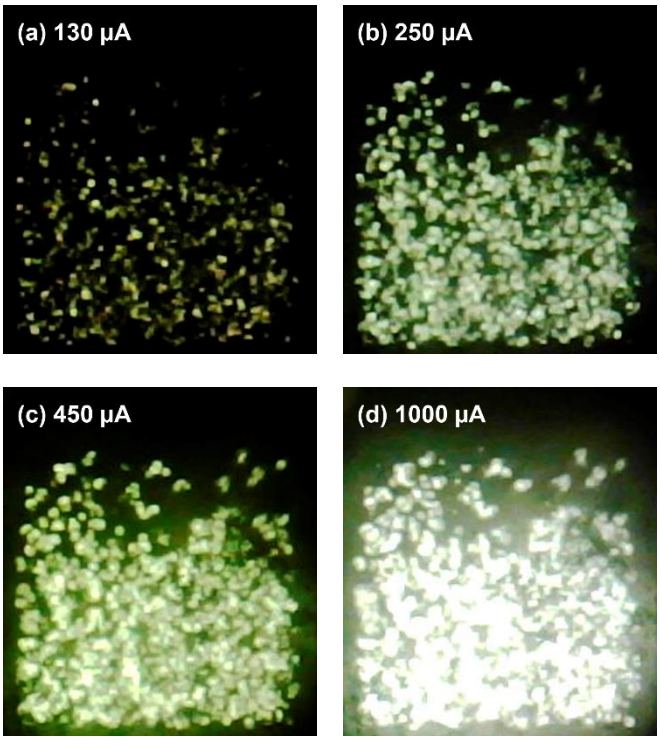

Figure 7. Glow pattern at 130 μA (a), 250 μA (b), 450 μA (c), 1000 μA (d) emission current levels.

Collection of emission sites was made for I = 220 μA. In fig. 8 the dependence of the number of registered emission sites on time was shown.

After the amount of registered emission sites reached a relatively stable level, we can assume that all the main emitting sites of the cathode were found. Then, each of the site was monitored to determine its maximum emissivity. After the output of the sum of the maximum brightness of the sites found at a relatively stable level, we can assume that all maximum brightness and currents are found.

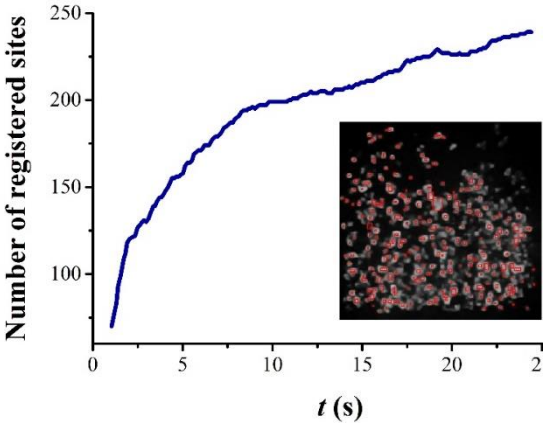

Figure 8. Dependence of the number of registered emission sites on time at current level of 220 μA.

The distribution of microscopic emission sites of the emitter is determined from these currents by the magnitude of the FEF (see Fig. 8b). The method of online calculation of local emission currents and FEFs of individual emission sites was described in detail in [19, 20]. It is based on the idea of the brightness of the emission site in the luminescence pattern as the weight coefficient of the current contribution of this site. Then, numerically solving the Fowler-Nordheim equation with respect to FEF for a given work function (for CNTs, it is 4.6 eV) and area emission of one emission center (was chosen equal to 200 nm^2 based on the ratio of the effective FEA and the number of centers found).

The values of the obtained local FEF correlate with the effective FEF (~ 1650).

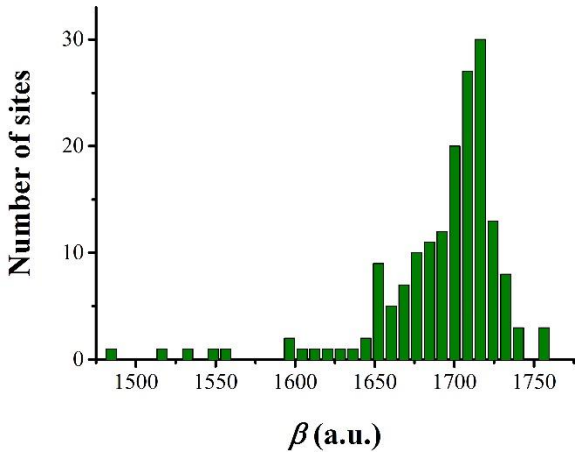

Figure 9. Histogram of the field enhancement factor distribution.

Figure 10 shows the result of the analysis of the emission site distribution over the cathode surface - the radial distribution diagram. Since the technique is designed for samples with circular substrates, and the sample holding diaphragm had a square hole, the analysis was performed for a circular zone inscribed in this square.

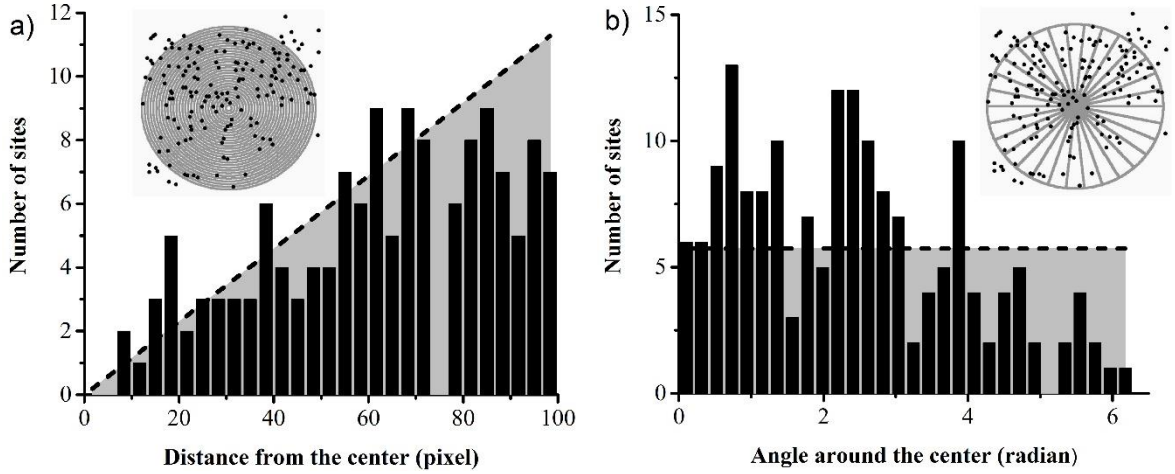

Figure 10. Chart of the emission site distribution along the radius (a) and angle (b).

Similarly, diagrams of the site distribution of brightness and a diagram of the distribution of total current loading of surface segments over the whole sample were obtained. Using these diagrams, the correlation coefficient R_{cor} and the covariance coefficient V_{cov} were calculated, which make it possible to estimate the ideality of the site distribution [19]. For this sample, they were: R_{cor} = 53%, V_{cov} = 63%. This numerical estimate allows directional optimization of the surface quality of the cathodes.

4. Conclusion

The paper presents a characterization of a sample of a multi-tip field cathode based on non-oriented CNTs grown on a multilayer substrate by the PECVD method. The developed system for testing and numerical characterization of the emission properties of field cathodes includes: a description of the sample activation process by high voltage, an assessment of the temporal stability of the emission current, as well as its dynamic characteristics when the voltage level changes, checking for compliance of the emission signal with the pure field emission mode, plotting fluctuation histograms effective parameters, the construction of the emission site distribution by the values of the local field enhancement factor and, finally, the estimate uniformity of emission sites distribution over the cathode surface and the level of their emission activity.

The constructed histograms of the distribution of microscopic emission sites by the magnitude of the local field enhancement factor showed good agreement with the effective value of this parameter. Despite the fact that the macroscopic effective parameters and local estimates of β are linked at the level of estimates of macroscopic and microscopic emission areas, the method of decomposing the effective β_{eff} into many local β has great prospects for understanding and analyzing the fundamental laws of operation of multi-tip field emitters.

References

[1] Ohkawa Y, Okumura T, Iki K, Okamoro H and Kawamoto S 2018 *31st Int. Vac. Nanoelectronic Conf.* Kyoto, Japan 09-13 july 40-41
[2] Yang Ch and Velásquez-García L F 2019 *J. Phys. D: Appl. Phys.* **52** 075301-1-9
[3] Rudyk N N, Il'in O I, Il'ina M V, Fedotov A A, Klimin V S and Ageev O A 2017 *J of Phys.: Conf. Series* **917** 082008-1-5
[4] Mavalankar A, Cameron J and Travish G 2017 *30th Int. Vac. Nanoelectronics Conf.* Regensburg, Germany 300-301
[5] Lin P-H, Sie C-L, Chen C-A, Chang H-C, Shih Y-T, Chang H-Y, Su W-J and Lee K-Y 2015 *Nanoscale Res. Lett.* **10** 297
[6] Chiu C-C, Tsai T-Y and Tai N-H 2006 *Nanotechnology* **17** 2840–4

[7] Bandurin D A, Kleshch V I, Smolnikova E A, Obronov I V, Nasibulin A G, Kauppinen E I and Obraztsov A N 2013 *J. of Nanoelectronics and Optoelectronics* **8** 114–118
[8] Pandey A, Prasad A, Moscatello J P, Engelhard M, Wang C and Yap Y K 2013 *ACS Nano* **7** 117–25
[9] Patra R, Singh A, Vankar V D, Ghosh S 2016 *Adv. Mater. Lett.* **7(10)** 771-776
[10] Li Y, Sun Y, Jaffray D A and Yeow J T W 2017 *Nanotechnology* **28** 155704 1-12
[11] Chubenko O, Baturin S S, Kovi K K, Sumant A V and Baryshev S V 2017 *ACS Appl. Mater. Interfaces* **9** 33229−3323
[12] Kopelvski M M, Galeazzo E, Peres H E M, Ramirez-Fernandez F J, Silva D A C and Dantas M O S 2016 *Measurement* **93** 208–214
[13] Zhao L, Chen Y, Zhang Z, Cao X, Zhang G, She J, Deng S, Xu N and Chen J 2018 *Sci. Reports* **8** 12294
[14] Popov E O, Kolosko A G, Filippov S V, Romanov P A and Fedichkin I L 2018 *Materials Today: Proceedings* **5** 13800–13806
[15] Kolosko A G, Popov E O, Filippov S V and Romanov 2015 *J of Vac.Sci. & Tech. B* **33** 03C104
[16] Kolosko A G, Popov E O, Filippov S V and Romanov P A 2014 *Technical Physics Letters* **40 5** 438–441
[17] Kolosko A G, Filippov S V, Romanov P A, Popov E O and Forbes R G 2016 *J of Vac.Sci. & Tech. B* **34** 041802
[18] Popov E O, Kolosko A G, Filippov S V, Fedichkin I L and Romanov P A 2015 *J of Vac.Sci. & Tech. B* **33**, 03C109
[19] Filippov S V, Popov E O, Kolosko A G and Vinnichek R N 2017 *Jour. of Phys.: Conf. Ser* **917** 092022
[20] Popov E O, Kolosko A G, Filippov S V and Terukov E I 2018 *J of Vac.Sci. & Tech. B* **36** 02C106